Fabrication and photocatalytic activity of high-efficiency visible-light-responsive photocatalyst ZnTe/TiO$_2$ nanotube arrays

Yutang Liu [a,b,1], Xilin Zhang [b,1], Ronghua Liu [b], Renbin Yang [a,*], Chengbin Liu [b,*], Qingyun Cai [b]

[a] College of Bioscience and Biotechnology, Hunan Agricultural University, Changsha 410128, People's Republic of China
[b] State Key Laboratory of Chemo/Biosensing and Chemometrics, Hunan University, Changsha 410082, People's Republic of China

ABSTRACT

A new ZnTe modified TiO$_2$ nanotube (NT) array catalyst was prepared by pulse potential electro-deposition of ZnTe nanoparticles (NPs) onto TiO$_2$ NT arrays, and its application for photocatalytic degradation of anthracene-9-carboxylic acid (9-AnCOOH) was investigated. The even distribution of ZnTe NPs was well-proportionately grown on the top surface of the TiO$_2$ NT while without clogging the tube entrances. Compared with the unmodified TiO$_2$ NT, the ZnTe modified TiO$_2$ NT (ZnTe/TiO$_2$ NT) showed significantly enhanced photocatalytic activity towards 9-AnCOOH under simulated solar light. After 70 min of irradiation, 9-AnCOOH was degraded with the removal ratio of 45% on the bare TiO$_2$ NT, much lower than 80%, 90%, and 100% on the ZnTe/TiO$_2$ NT with the ZnTe NPs prepared under the pulsed "on" potentials of −0.8, −1.0, and −2.0 V, respectively. The increased photodegradation efficiency mainly results from the improved photocurrent density as results of enhanced visible-light absorption and decreased hole–electron recombination due to the presence of narrow-band-gap p-type semiconductor ZnTe.

© 2011 Elsevier Inc. All rights reserved.

1. Introduction

Recently, titanium dioxide (TiO$_2$), with low cost, chemical inertness, and photostability, has been extensively studied for environmental protection due to its excellent photocatalytic activity for the degradation of organic pollutant [1–3]. Among the well-investigated TiO$_2$ nanostructured materials, vertically aligned TiO$_2$ NT array has been paid particular attention because of the high orientation, tunable mesopore size, large internal surface area, easy to recycle as well as excellent electron percolation pathways, and thus it can greatly promote vectorial charge transfer between interfaces [4]. However, the practical application is still limited by the large band gap of TiO$_2$ (3.0 and 3.2 eV for the rutile and anatase phases, respectively) that only matches the 4–5% UV light of the solar spectrum. Sensitizing n-type TiO$_2$ NT with p-type active materials such as Cu and Cu$_2$O [5–7] is one of efficient ways to fabricate TiO$_2$-based catalysts with extended absorption in the visible light and enhanced photocatalytic activity. The separation of photoinduced hole–electron pairs can be accelerated by the potential difference at the p–n heterojunction interface. Moreover, the guest semiconductor with narrow band gap can facilitate the extended absorption in the visible light.

Solar cells based on *II–VI* semiconductors (*II*=Zn, Cd, Hg, *VI*=S, Se, Te) are among the leading candidates for low-cost photovoltaic conversion of solar energy [8–11] due to their high absorption coefficients and therefore the low material consumption for their production. Choi and co-workers [12] used dip-coating to deposit CdTe nanoparticles, resulting in even distribution of CdTe nanoparticles inside the pores of TiO$_2$ nanotubes without clogging the surface of TiO$_2$ nanotubes. Among the semiconductors, ZnTe possesses a narrow band gap of 2.23–2.28 eV, and has been used as a p-type semiconductor for the construction of heterojunction photovoltaic cells [13]. The higher conduction band (CB) and valence band (VB) of ZnTe indicate the easy formation of p–n heterojunction interface between ZnTe and TiO$_2$. In this respect, ZnTe is expected to be a promising material for photocatalysis. However, to our best knowledge, there is no report about ZnTe-sensitized TiO$_2$ NT through pulse electrodeposition technique.

ZnTe can be prepared by electrodeposition technique [14–16], which is attractive due to its simplicity and low cost. Recently, a pulsed electrodeposition technique, based on a multipulse sequence of current densities or potentials of equal amplitude and duration, has been proposed for the preparation of metal or metal oxide nanocrystals [17–18]. By this technique, nucleation and growth of the crystallites can be controlled by varying the pulse amplitude and duration, and thus, it is helpful to obtain

monodisperse nanostructured materials. 9-AnCOOH is an aromatic compound with a similar structure to potential environmental pollutants. In this work, ZnTe NPs were deposited onto TiO_2 NT by using pulse potential deposition, and the photocatalysis of the $ZnTe/TiO_2$ NT towards 9-AnCOOH were investigated.

2. Experimental sections

2.1. Chemicals and materials

Titanium foil (99.8%, 250 μm thickness) was purchased from Aldrich (Milwaukee, WI), 9-AnCOOH was obtained from Johnson Matthey Alfa AESAR. Other reagents were of the highest commercially available quality and purified before use. Deionized water was used for preparation of all aqueous solutions.

2.2. Preparation of TiO_2 NT arrays

TiO_2 NT arrays were prepared according to our previous work [19]. Prior to anodization, titanium ribbons were ultrasonically cleaned in acetone and ethanol. The cleaned titanium ribbon was anodized at 15 V in an electrolyte containing 0.1 M NaF and 0.5 M $NaHSO_4$ at room temperature for 3 h in a two-electrode system with a platinum cathode, resulting in the TiO_2 NT array with a pore size of 90–100 nm, a length of 320 nm and an efficient electrode area of 3 cm × 1 cm on each side [19,20].

2.3. Preparation of ZnTe modified TiO_2 NT arrays

A typical three-electrode electrochemical cell (IM6ex) was equipped with a Pt wire as the counter electrode, a saturated calomel electrode (SCE) as the reference electrode and a TiO_2 NT array as the working electrode. A solution containing 25 mM $ZnSO_4$ and 5 mM Na_2TeO_3 was used for electrodeposition. Pulsed potentials were applied to the cathode, where the "on" potential was −0.8, −1.0, and −2.0 V, respectively; the "off" potential was −0.000001 V. The "on" and "off" times were 0.2 and 1.0 s, respectively, and the number of pulse sequence is 1200. After deposition, the ZnTe modified TiO_2 NT arrays were washed several times with deionized water, obtaining the $ZnTe/TiO_2$ NT. The electrodeposition process was illustrated in Scheme 1. At last, all the samples were annealed in nitrogen atmosphere at 300 °C for 3 h.

2.4. Characterization of $ZnTe/TiO_2$ NT arrays

The morphologies of the unmodified and the modified TiO_2 NT arrays were investigated by using a field emission scanning electron microscope (FESEM, Hitachi, model S-4800). Energy

dispersive X-ray (EDX) spectrometer fitted to electron microscopes was used for elemental analysis. The crystal phases of the resulting TiO_2 array samples were determined by an X-ray diffractometer with Cu-Kα radiation (XRD, M21X, MAC Science Ltd., Japan). UV–vis diffuse reflectance spectra (DRS) were recorded on a Cary 300 Conc UV–visible spectrophotometer with an integrating sphere. Photoluminescence (PL) spectra were recorded using Hitachi F-2500 fluorescence spectrophotometer at an excitation wavelength of 270 nm.

2.5. Photoelectrochemical measurements

Photoelectrochemical studies were carried out using a three-electrode configuration with TiO_2 NT as the working electrode, Pt foil as the counter electrode and a saturated calomel electrode (SCE) as the reference electrode in 0.5 M Na_2SO_4 solution. A 500 W xenon arc lamp (CHF-XQ-500W, Beijing Changtuo Co. Ltd.) served as the simulated solar light source (280–2000 nm) with the photon flux of 100 mW cm^{-2} measured by NOVA Oriel 70260 with a thermodetector. Photocurrents were recorded by an electrochemical working station (CH Instruments, Model CHI 660B).

2.6. Photocatalytic degradation of 9-AnCOOH

The photoelectrocatalysis degradation experiments were carried out under stirring in a quartz beaker equipped with a three-electrode system including TiO_2 NT with total active area of 6.0 cm^2 as the photo-anode, Pt foil electrode as the cathode, and SCE as the reference electrode. During photocatalysis degradation, the electrodes were vertically placed in the quartz beaker containing 60 mL of a mixed aqueous solution of 9-AnCOOH (10 mg L^{-1}) and sodium sulfate as an electrolyte (0.05 M). A 500 W xenon arc lamp served as the light source. During the reaction, the variation of the concentration of 9-AnCOOH in the solution was traced by a UV–visible spectrophotometer (Cary 300, Varian, USA).

3. Results and discussion

3.1. Morphology of the TiO_2 NT arrays

The surface morphologies of the TiO_2 NT are shown in Fig. 1. The unmodified TiO_2 NT is composed of high-density, well-ordered, and uniform TiO_2 nanotubes with length of about 320 nm, pore sizes ranging from 90 to 100 nm, and wall thickness of about 5 nm (Fig. 1a). ZnTe nano-crystallites are efficiently deposited onto the top surface of the highly oriented TiO_2 NT arrays, and all of the nano-crystallites are well-proportionedly grown on the TiO_2 NT (the corresponding enlarged drawings were
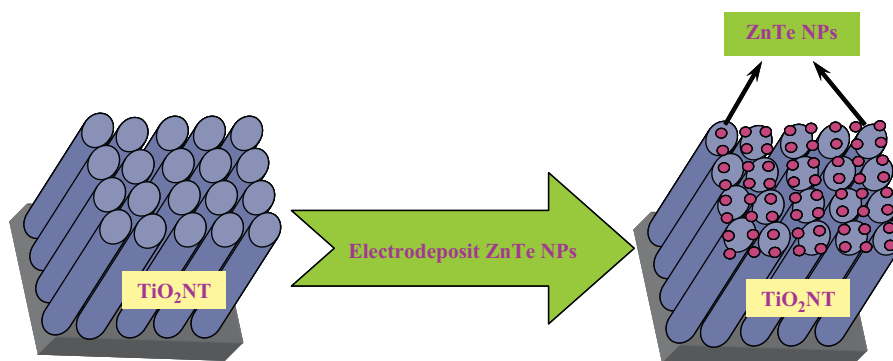
Scheme 1. Schematic illustration showing the electrodeposition of ZnTe on TiO_2 NT arrays.
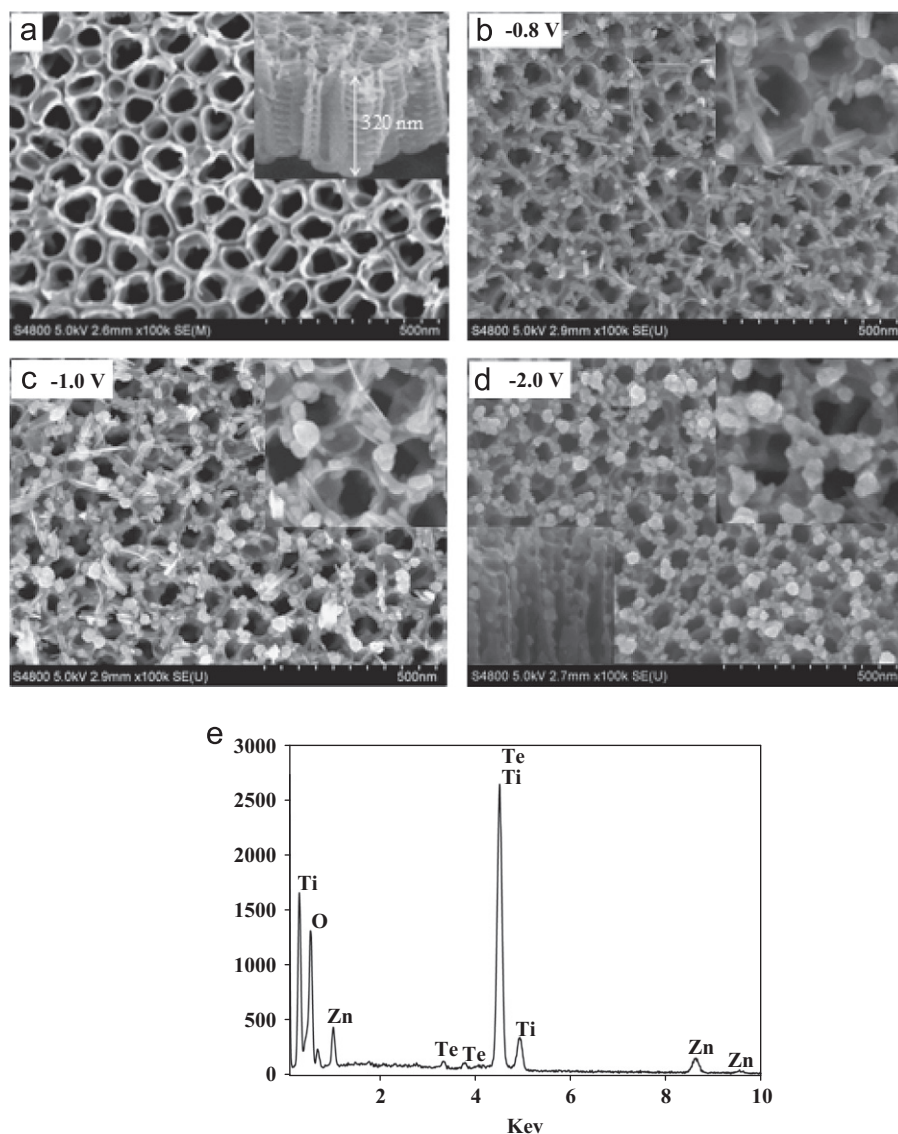
Fig. 1. Surface-view SEM images of: (a) unmodified TiO_2 NT, (b), (c), and (d) ZnTe/TiO_2 NT prepared under -0.8, -1.0, and -2.0 V, respectively. The insets in (a) (unmodified TiO_2 NT) and (d) (ZnTe/TiO_2 NT$_{-2\,V}$) are the corresponding cross-section image, the other insets are the corresponding enlarged drawings. (e) The EDX pattern of the ZnTe/TiO_2 NT$_{-0.8\,V}$ arrays.

shown in the top right corner of each figures), which could help minimize the clogging at the tube entrances (Fig. 1b–d). Moreover, as shown in the cross-section of SEM images (see the inset in the left bottom of Fig. 1d), a small quantity of ZnTe NPs was deposited onto the inner of the TiO_2 nanotubes without clogging the channels. Therefore, the rational distribution of ZnTe nano-crystallites on the top surface of the tubes would favor light absorption. The morphologies of ZnTe nano-crystallites are well-related to the pulsed "on" potentials. As shown in Fig. 1b, ZnTe crystalline strips were obviously formed under the applied "on" potential of -0.8 V (ZnTe/TiO_2 NT$_{-0.8\,V}$), while ZnTe NPs coexisted with less strips were observed under -1.0 V (ZnTe/TiO_2 NT$_{-1.0\,V}$) (Fig. 1c). When the "on" potential was added to -2.0 V (ZnTe/TiO_2 NT$_{-2.0\,V}$), all of the ZnTe crystallites changed to nanoparticle (Fig. 1d). This result indicates that higher voltage will be favorable for the formation of ZnTe NPs. The composition of the samples was determined by energy dispersive X-ray spectroscopy (EDX) (Fig. 1e). The EDX result shows that the modified TiO_2 NT contains the elements of O, Zn, Te, and Ti, and the loading (wt%) and the molar ratio of Zn and Te are shown in Table 1. The sample obtained under -2.0 V has the molar ratio proximal to 1, in accordance with the intrinsic molar component of ZnTe.

Table 1
The Zn, Te contents, and molar percentage under different prepared potentials.

Samples	Voltage (V)	Zn loading (wt%)	Te loading (wt%)	Molar ratio of Zn to Te
B	-0.8	0.22	0.37	1.240
C	-1.0	0.18	0.29	1.238
D	-2.0	0.20	0.36	1.074

3.2. XRD spectra analysis

The XRD spectra of both the unmodified TiO_2 NT (Fig. 2a) and the ZnTe/TiO_2 NT (Fig. 2b) exhibit the characteristic diffraction peaks of anatase phase at $2\theta=25.5°$, $38.6°$, $48.1°$, and $54.1°$ corresponding to the lattice distance of 3.50, 2.34, 1.89 and 1.70 Å, respectively. Compared with the unmodified TiO_2 NT, the main diffraction peaks of ZnTe/TiO_2 NT at $2\theta=25.2°$, $41.9°$, and $49.5°$ are attributed to the (111), (220), and (311) planes, respectively, with the corresponding lattice constant values of 3.51, 2.16, and 1.84 Å, indicating the existence of the cubic
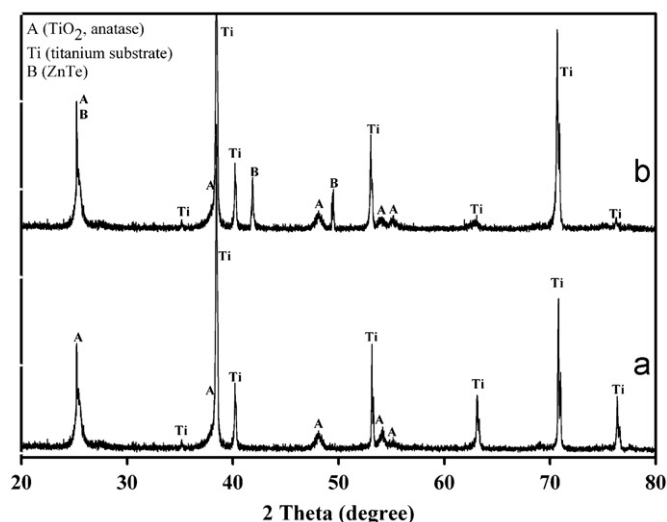
Fig. 2. XRD patterns of (a) unmodified TiO$_2$ NT and (b) ZnTe/TiO$_2$ NT$_{-0.8 V}$.

Table 2
Relative peak intensities (RPI) of ZnTe under different potentials.

Samples	RPI 2θ		
	25.2	41.9	49.5
ZnTe/TiO$_2$ NT$_{-0.8 V}$	230	100	75
ZnTe/TiO$_2$ NT$_{-1.0 V}$	250	115	80
ZnTe/TiO$_2$ NT$_{-2.0 V}$	300	130	100

Fig. 3. DRS spectra of the unmodified TiO$_2$ NT and ZnTe/TiO$_2$ NT arrays.

Fig. 4. The photocurrent densities obtained on the unmodified TiO$_2$ NT and ZnTe/TiO$_2$ NT in 0.05 M Na$_2$SO$_4$ solution.

crystalline ZnTe NPs [15]. The ZnTe/TiO$_2$ NT samples prepared under the "on" potentials of -0.8, -1.0, and -2.0 V (ZnTe/TiO$_2$ NT$_{-0.8 V}$, ZnTe/TiO$_2$ NT$_{-1.0 V}$, and ZnTe/TiO$_2$ NT$_{-2.0 V}$) were compared in terms of the relative peak intensities (RPI) of ZnTe, and the results are shown in Table 2. As can been seen, the RPI of ZnTe increased with increasing the electrodeposition potential, suggesting an increased crystallinity of ZnTe NPs deposited at a much higher voltage.

3.3. DRS spectra analysis

The UV–vis diffuse reflectance spectra of unmodified TiO$_2$ NT and ZnTe/TiO$_2$ NT are shown in Fig. 3. There are two characteristic absorption peaks of TiO$_2$. The first one at about 380 nm results from the absorption of the trapped hole, and the other one at around 470–600 nm is due to the absorption of the trapped electron at the Ti^{4+} center [21]. Compared with the unmodified TiO$_2$ NT, all of ZnTe/TiO$_2$ NT arrays exhibit increased light absorption intensity in the visible region. Moreover, the absorption edge of ZnTe/TiO$_2$ NT arrays is shifted from 580 (the neat TiO$_2$ NT) to 629, 658, and 687 nm depending on the applied pulsed potentials for ZnTe preparation, which is due to the combination of a narrow band gap of ZnTe with a wide band gap of TiO$_2$ NT responsible for the improved spectra absorption capability of TiO$_2$ NT. These suggest that the ZnTe/TiO$_2$ NT can make more efficient use of visible light compared with the unmodified TiO$_2$ NT, particularly for the ZnTe/TiO$_2$ NT$_{-2.0 V}$ sample where the ZnTe NPs exhibit better crystallinity than that in other cases.
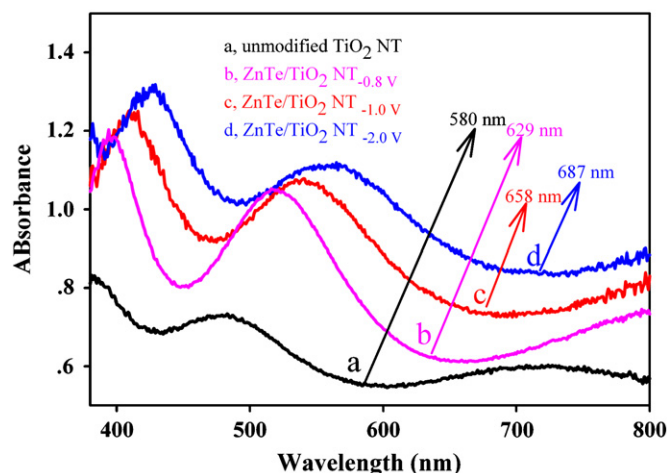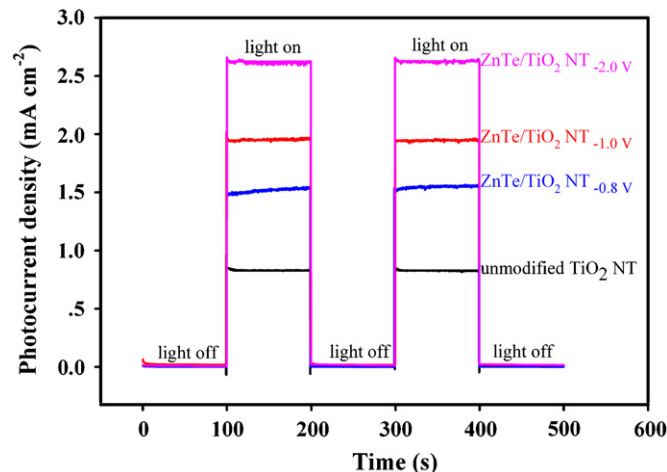
3.4. Photoelectrochemical properties of the ZnTe/TiO$_2$ NT arrays

The photoelectrochemical response of the samples was analyzed under simulated solar light irradiation cutting off infrared light under room temperature without bias potential, and the pH is neutral. The photocurrent is from the photogenerated electrons in the conducting bands of ZnTe and TiO$_2$ with leaving holes in their valence bands under Xe-light irradiation. The curves shown in Fig. 4 were collected from TiO$_2$ NT and ZnTe/TiO$_2$ NT in a 0.05 M Na$_2$SO$_4$ solution. The dark current of unmodified TiO$_2$ NT is near zero. The photocurrent densities of ZnTe/TiO$_2$ NT$_{-0.8 V}$, ZnTe/TiO$_2$ NT$_{-1.0 V}$, and ZnTe/TiO$_2$ NT$_{-2.0 V}$ are 1.51, 1.92, and 2.68 mA cm^{-2}, about 1.8, 2.3, and 3.3 times larger than that of the unmodified TiO$_2$ NT (0.82 mA cm^{-2}), respectively. This represents that the increases in photocurrent are mainly attributed to the ZnTe NPs. The ZnTe/TiO$_2$ NT$_{-2.0 V}$ is the most effective one to transfer photogenerated charges. On the one hand, this sample greatly improved the utilization of visible light; on the other hand, the good crystallinity of the sample is favorable to the separation and transport of charges. Therefore, ZnTe/TiO$_2$ NT$_{-2.0 V}$ is expected to exhibit the minimal recombination of photogenerated charges during photocatalysis and to be a good photocatalyst for organic pollutant degradation.

3.5. Photoluminescence spectra analysis

The PL emission spectra have been widely used to investigate the efficiency of charge carrier trapping, immigration and transfer, and to understand the fate of electron−hole pairs in semiconductor particles [22]. In Fig. 5, the modified and unmodified TiO$_2$ NT arrays exhibit similar broad PL emission bands, whereas the PL intensity decreases with the order: unmodified TiO$_2$ NT < ZnTe/TiO$_2$ NT$_{-0.8\ V}$ < ZnTe/TiO$_2$ NT$_{-1.0\ V}$ < ZnTe/TiO$_2$ NT$_{-2.0\ V}$. This implies that the presence of ZnTe NPs reduces the possibility

Fig. 5. PL spectra of unmodified TiO$_2$ NT and ZnTe/TiO$_2$ NT arrays.

of the electron−hole recombination that leads to the decreased PL intensity, especially for ZnTe/TiO$_2$ NT$_{-2.0\ V}$.

3.6. Photocatalytic degradation 9-AnCOOH

The direct photolytic (DP) process without photocatalyst and photocatalytic (PC) process were performed under simulated solar light. Obviously, a much higher efficiency was achieved through the PC process than through the DP process (Fig. 6a). All the ZnTe/TiO$_2$ NT samples exhibit a greatly enhanced photodegradation activity than that in the case of the bare TiO$_2$ NT. For example, for 70 min of illumination, 9-AnCOOH was degraded with the removal ratio of 45% on the bare TiO$_2$ NT, much lower than 80%, 90%, and 100% on the ZnTe/TiO$_2$ NT$_{-0.8\ V}$, ZnTe/TiO$_2$ NT$_{-1.0\ V}$, and ZnTe/TiO$_2$ NT$_{-2.0\ V}$, respectively. Again, the degradation efficiency of ZnTe/TiO$_2$ NT is well-related to the formation conditions of ZnTe, and the ZnTe/TiO$_2$ NT$_{-2.0\ V}$ shows the highest photocatalytic rate resulting from the synergetic effects of light absorption and charge separation. Fig. 6b shows UV−vis spectra of 9-AnCOOH in situ degraded on the ZnTe/TiO$_2$ NT$_{-2.0\ V}$ under the simulated solar light, depicting that the characteristic adsorption peaks of 9-AnCOOH drastically decrease and finally disappear within 70 min of irradiation.

3.7. Photocatalytic mechanism

Scheme 2 illustrates the transfer processes of photogenerated electrons and holes in the catalytic system of ZnTe/TiO$_2$ NT. ZnTe is a p-type semiconductor, and its electrodeposition onto TiO$_2$ NT
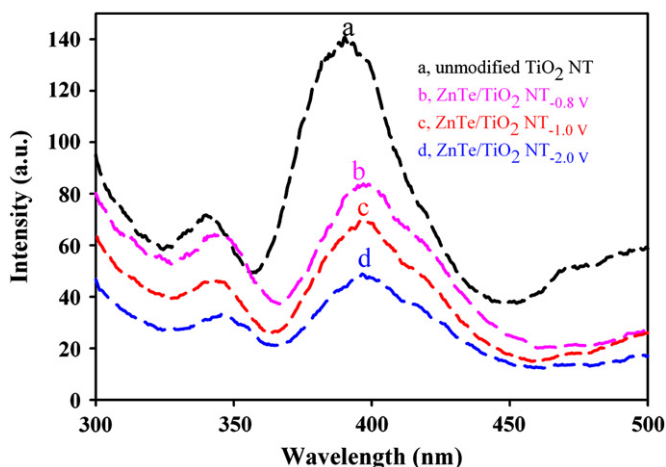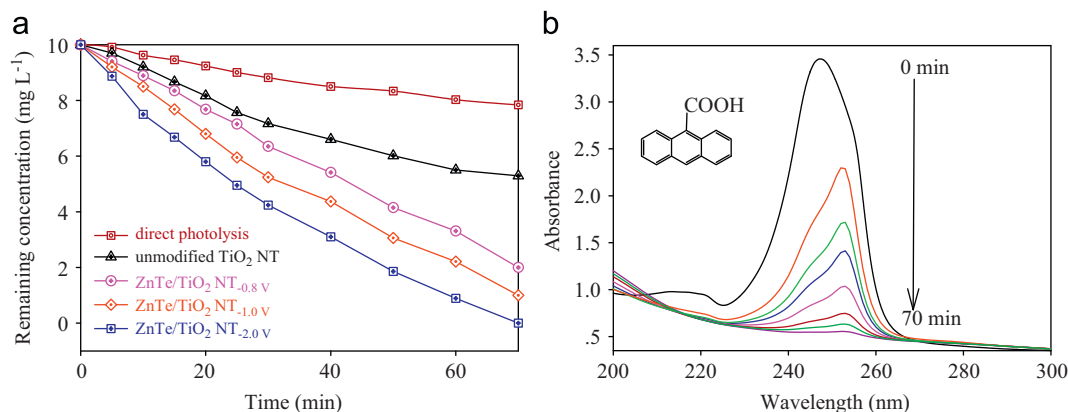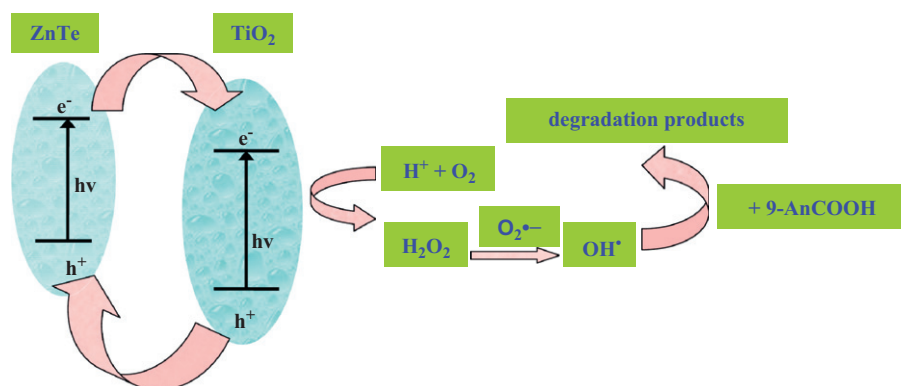

Fig. 6. (a) Irradiation time-dependent degradation rate of 9-AnCOOH during direct photolytic (DP) process without photocatalyst and photocatalytic (PC) process on unmodified TiO$_2$ NT and ZnTe/TiO$_2$ NT. (b) In situ UV–visible determination of 9-AnCOOH photodegradation on the ZnTe/TiO$_2$ NT$_{-2.0\ V}$ electrode.

Scheme 2. Illustrative diagrams of the electron and hole transfer in ZnTe/TiO$_2$ NT and the mechanism of photocatalysis degradation.

arrays leads to the formation of p–n junction between them. Under simulated solar light irradiation, electrons of ZnTe NPs and TiO_2 NT were excited by visible and UV light, respectively, from the valence band (VB) to the conduction band (CB). The photo-generated electrons transfer from ZnTe CB to the TiO_2 CB and react with electron acceptors such as O_2 adsorbed on the TiO_2 NT or dissolved in water, reducing it to superoxide radical anion $O_2^{\cdot-}$, which combines with H^+ form hydrogen peroxide (H_2O_2), and H_2O_2 can react with $O_2^{\cdot-}$, reducing to hydroxyl radicals ($^{\cdot}OH$), whereas the photogenerated holes move from the TiO_2 VB to the ZnTe VB, and accumulated in the ZnTe VB can react with H_2O to form hydroxyl to generate radicals ($^{\cdot}OH$). Being a very strong oxidizing agent, the resulting $^{\cdot}OH$ radical can oxidize most of organic compounds to the mineral end-products.

4. Conclusions

A new ZnTe/TiO_2 NT catalyst was prepared by pulse electro-deposition of ZnTe NPs onto TiO_2 NT arrays. Compared with the unmodified TiO_2 NT, the ZnTe modified TiO_2 NT showed remarkably increased photocurrent density, and thus significantly enhanced photocatalytic activity in the degradation of 9-AnCOOH, indicating a promising application in practical systems.

Acknowledgments

References

[1] H.J. Liu, G.G. Liu, Q.X. Zhou, J. Solid State Chem. 182 (2009) 3238–3242.
[2] C.Y. Yang, W.D. Wang, Z.C. Shan, F.Q. Huang, J. Solid State Chem. 182 (2009) 807–812.
[3] D. Jiang, Y. Xu, D. Wu, Y.H. Sun, J. Solid State Chem. 181 (2008) 593–602.
[4] S. Rani, S.C. Roy, M. Paulose, O.K. Varghese, G.K. Mor, S. Kim, S. Yoriya, T.J. LaTempa, C.A. Grimes, Phys. Chem. Chem. Phys. 12 (2010) 2780–2800.
[5] G.K. Mor, O.K. Varghese, R.H.T. Wilke, S. Sharma, K. Shankar, T.J. Latempa, K.S. Choi, C.A. Grimes, Nano Lett. 8 (2008) 1906–1911.
[6] Q. Wang, K. Zhu, N.R. Neale, A.J. Frank, Nano Lett. 9 (2009) 806–813.
[7] Y. Hou, X.Y. Li, X.J. Zou, X. Quan, G.H. Chen, Environ. Sci. Technol. 43 (2009) 858–863.
[8] D.A. Cusano, Solid State Electron. 6 (1963) 217–218.
[9] M. Afzaal, P. O'Brien, J. Mater. Chem. 16 (2006) 1597–1602.
[10] A. Kongkanand, K. Tvrdy, K. Takechi, M. Kuno, P.V. Kamat, J. Am. Chem. Soc. 130 (2008) 4007–4015.
[11] L. Wonjoo, L. Jungwoo, L. Sangjin, Y. Whikun, H. Sung-Hwan., C.Byung Won, Appl. Phys. Lett. 92 (2009) 153510–153513.
[12] J.A. Seabold, K. Shankar, R.H.T. Wilke, M. Paulose, O.K. Varghese, C.A. Grimes, K.S. Choi., Chem. Mater. 20 (2008) 5266–5273.
[13] P.V. Meyers, C.H. Liu, T.J. Frey, US Patent 4710589, 1987.
[14] M. Neumann-Spallart, C. Königstein, Thin Solid Films 265 (1995) 33–39.
[15] N.B. Chaure, R. Jayakrishnan, J.P. Nair, R.K. Pandeyy, Semicond. Sci. Technol. 12 (1997) 1171–1175.
[16] T. Gandhi, K.S. Raja, M. Misra, Thin Solid Films 517 (2009) 4527–4533.
[17] S.S. Kim, S.I. Na, J. Jo, D.Y. Kim, Y.C. Nah, Appl. Phys. Lett. 93 (2008) 073307–073310.
[18] C. Coutanceau, A.F. Rakotondrainibé, A. Lima, E. Garnier, S. Pronier, J.-M. Léger, C. Lamy, J. Appl. Electrochem. 34 (2004) 61–66.
[19] Y.T. Liu, R.H. Liu, C.B. Liu, S.L. Luo, L.X. Yang, F. Sui, Y.R. Teng, R.B. Yang, Q.Y. Cai, J. Hazard. Mater. 182 (2010) 912–918.
[20] Q.Y. Cai, M. Paulose, O.K. Varghese, C.A. Grimes, J. Mater. Res. 20 (2005) 230–234.
[21] D.W. Bahnemann, R. Dillert, P.K.J. Robertson, in: A.I. Kokorin, D.W. Bahnemann (Eds.), Photocatalysis, VSP BS, Eindhoven, The Netherlands, 2003 Chapter 7.
[22] H. Yamashita, Y. Ichihashi, S.G. Zhang, Y. Matrumura, Y. Souma, T. Tatsumi, M. Anpo, Appl. Surf. Sci. 305 (1997) 121–122.